NNLO QCD corrections to the polarized top quark decay $t(\uparrow) \to X_b + W^+$

A. Czarnecki,[1] S. Groote,[2] J. G. Körner,[3] and J. H. Piclum[4]

[1]*Department of Physics, University of Alberta, Edmonton, Alberta T6G 2E1, Canada*
[2]*Loodus- ja täppisteaduste valdkond, Füüsika Instituut,
Tartu Ülikool, W. Ostwaldi 1, 50411 Tartu, Estonia*
[3]*Institut für Physik, Johannes-Gutenberg-Universität, Staudinger Weg 7, 55099 Mainz, Germany*
[4]*Theoretische Physik 1, Naturwissenschaftliche-Technische Fakultät,
Universität Siegen, 57068 Siegen, Germany*

We compute the next-to-next-to-leading order (NNLO) QCD corrections to the decay $t(\uparrow) \to X_b + W^+$ of a polarized top quark. The spin-momentum correlation in this quasi two-body decay is described by the polar angle distribution $d\Gamma/d\cos\theta_P = \frac{\Gamma}{2}(1 + P_t\alpha_P\cos\theta_P)$, where P_t is the polarization of the top quark and α_P denotes the asymmetry parameter of the decay. For the latter we find $\alpha_P^{\text{NNLO}} = 0.3792 \pm 0.0037$.

I. INTRODUCTION

The number of single top quark events reported by the LHC Collaborations ATLAS and CMS in Run 1 and 2 is ever increasing. More and more single top quark events are being seen at the LHC [1–4]. The present situation concerning both ATLAS and CMS results on single top production is nicely summarized in a review article by N. Faltermann [5]. After Run 3 the LHC will operate in the high luminosity mode with a projected total luminosity of 3 ab^{-1}, which corresponds to approximately 10^9 single top quark events. In the dominating t-channel process, which is a weak production process, single top quarks are produced with a large longitudinal polarization $P_t \simeq 0.9$ in the direction of the spectator jet in the top quark rest frame, and a slightly smaller polarization of $P_t \simeq 0.8$ for antitop quarks [6–9].[1] Since the top quark decays so rapidly, it retains its polarization from birth when it decays. The dominant decay mode is the quasi two-body mode $t(\uparrow) \to X_b + W^+$ mediated by the quark level transition $t \to b$ proportional to the CKM matrix element $V_{tb} \approx 1$.

In this paper we study top quark polarization effects in the quasi two-body decay $t(\uparrow) \to X_b + W^+$ at next-to-next-to-leading order (NNLO) in QCD. The NNLO results are obtained in the form of a power series expansion in terms of

the ratio $x = m_W/m_t$, where m_W and m_t are the masses of the W boson and the top quark, and we include terms up to x^{10}. This analysis can be considered to be complementary to the decay part of the recent numerical NNLO evaluation of polarized top production and decay [11,12].

Since the decay is weak, the top quark is self-analyzing. The angular decay distribution reads

$$\frac{1}{\Gamma}\frac{d\Gamma}{d\cos\theta_P} = \frac{1}{2}(1 + P_t\alpha_P\cos\theta_P), \tag{1}$$

where θ_P is the angle between the polarization direction of the top quark and the momentum direction of the W^+ (see Fig. 1). The analyzing power for the polarization of the decay is given by the asymmetry parameter α_P where, at leading order (LO), one has $\alpha_P^{\text{LO}} = (1 - 2x^2)/(1 + 2x^2) = 0.398$. Here and throughout this paper we set the bottom quark mass to zero.

The measurements suggested here require the reconstruction of the momentum direction of the W boson, which is not simple experimentally. However, the experimentalists have

---

[1]Close to maximal values of the polarization of top quarks can be achieved with moderate tuning of the longitudinal beam polarization at the ILC (see, e.g., Ref. [10]).
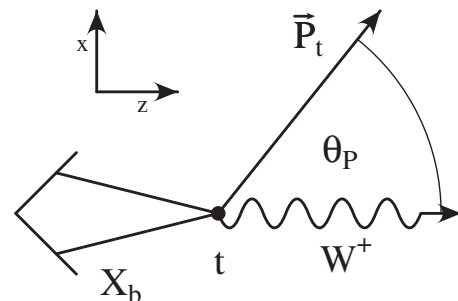
FIG. 1. Definition of the polar angle θ_P in the decay $t(\uparrow) \to X_b + W^+$.

devised sophisticated tools to reconstruct the W-boson momentum direction for their analysis of the helicity fractions in unpolarized top quark decays which can also be used in this analysis.

This paper is organized as follows. In Sec. II we outline the calculational methods used to obtain our result. In Sec. III we provide a numerical analysis of the decay rate and the asymmetry parameter. A summary and outlook are given in Sec. IV. Analytical results for the decay rate can be found in the Appendix.

II. CALCULATION

Our calculation follows the approach used in Refs. [13–15] for the calculation of the total unpolarized decay rate and in Ref. [16] for the so-called helicity fractions of the W boson. Using the optical theorem, we compute the top-quark decay width from the imaginary part of self-energy diagrams,

$$\Gamma = \frac{1}{m_t} \text{Im}(\Sigma_t), \qquad (2)$$

where Σ_t is computed from one-particle irreducible self-energy diagrams of the top quark. We sum over the spin degrees of freedom of the W boson; i.e., we do not specify its helicity components as has been done in Ref. [16]. Thus, we use the unitary gauge form for the spin sum,

$$\sum_{m=\pm,L} \varepsilon^\mu(m)\varepsilon^\nu(m) = \mathbb{P}^{\mu\nu} = -g^{\mu\nu} + \frac{q^\mu q^\nu}{m_W^2}, \qquad (3)$$

which enters our calculation in the numerator of the W-boson propagator. Here q is the momentum of the W^+. At LO we have $q = p_t - p_b$, where p_t and p_b are the momenta of the top and bottom quark, respectively.

It is clear that the polar angle distribution is sensitive to the longitudinal polarization vector of the top quark, $s_t^{\ell,\mu}$. We have

$$\Sigma_t = \text{tr}((\not{p}_t + m_t)\not{s}_t^\ell \gamma_5 \Sigma), \qquad (4)$$

where $i\Sigma$ is the sum of the top-quark self-energy diagrams. In the rest frame of the top quark, the polarization vector reads $s_t^{\ell,\mu} = (0; 0, 0, 1)$; i.e., the three-dimensional polarization vector points in the direction of the momentum of the W boson (z direction in Fig. 1). For our calculation we require a covariant representation of the longitudinal polarization four-vector s_t^ℓ, which is given by

$$s_t^{\ell,\mu} = \frac{1}{|\vec{q}|} \left(q^\mu - \frac{p_t \cdot q}{m_t^2} p_t^\mu \right), \qquad (5)$$

where $|\vec{q}| = \sqrt{q_0^2 - q^2}$. The polarization four-vector $s_t^{\ell,\mu}$ can be seen to satisfy $p_t \cdot s_t^\ell = 0$ and $s_t^\ell \cdot s_t^\ell = -1$, where we use the fact that $p_t \cdot q = m_t q_0$ in the rest system of the top quark. Just as in the case of the helicity fractions, we find that

due to the polarization vector we have to deal with the modulus of the W momentum three-vector in the denominator of the expressions for the self-energy diagrams.

There are 38 three-loop diagrams altogether. Since we use the unitary gauge for the W boson, there is no need to include Goldstone bosons in the Feynman diagrams. For the gluons we use the covariant R_ξ gauge with the spin sum $\mathbb{P}^{\mu\nu}(R_\xi) = -g^{\mu\nu} + \xi k^\mu k^\nu / k^2$, where ξ is an arbitrary gauge parameter. We have checked that the gauge-parameter dependence cancels in the final result. Since we only require traces involving an even number of γ_5 matrices, we can work with a naively anticommuting γ_5 [17,18].

After setting the bottom-quark mass to zero, the Feynman integrals corresponding to the top-quark self-energy diagrams depend on two scales: the hard scale m_t and the soft scale m_W. We then employ the method of regions (see, e.g., Ref. [19]) to construct an expansion around the limit where the ratio $x = m_W/m_t$ of the two scales tends to zero. Here, we have to consider two regions for each loop momentum (the loop momenta are chosen to be the momenta of the gluons and the W boson). In the so-called hard region, all components of a loop momentum k scale like the hard scale $k^\mu \sim m_t$ for $\mu \in \{0, 1, 2, 3\}$ and in the so-called soft region all components scale like the soft scale $k^\mu \sim m_W$. In each region we then expand the integrand according to the scaling of all loop momenta. If the momentum of a gluon is soft, the corresponding loop integral becomes scaleless and is set to zero in dimensional regularization. We are therefore left with only two contributions for each integral: one where all loop momenta are hard and one where the gluon momenta are hard, but the momentum of the W boson is soft.

This expansion also makes it easier to deal with the unwieldy normalization factor $1/|\vec{q}|$ appearing in the covariant representation (5). In the hard region, we can express it in terms of a power series in $1/N^2$, where $N = (p_t + q)^2 - m_t^2 = 2p_t q + q^2$ is the denominator of a top-quark propagator with momentum $p_t + q$. Again using $p_t \cdot q = m_t q_0$, we find

$$4m_t^2 |\vec{q}|^2 = (N^2 - 2q^2 N + q^4 - 4m_t^2 q^2), \qquad (6)$$

which then leads to the expansion [16]

$$\frac{1}{|\vec{q}|} = \frac{2m_t}{N} \sum_{i=0}^{\infty} \binom{2i}{i} \left(\frac{2q^2 N - q^4 + 4m_t^2 q^2}{4N^2} \right)^i. \qquad (7)$$

In our calculation of the Feynman diagrams, we are only interested in the imaginary part due to a cut through the W-boson line. Thus, we can replace q^2 by m_W^2 in Eq. (7). The series is then truncated at the desired order in x.

In the soft region, it is not possible to construct an expansion of $|\vec{q}|$, since $|\vec{q}|^2 = q_0^2 - m_W^2$ and $q_0 \sim m_W$ in the soft region. However, in this region the loop containing the W boson factorizes from the remaining diagram due to the expansion. Therefore, the only integrals that have to be

modified are one-loop massive tadpole integrals, which are relatively simple.

After the expansion, all remaining integrals depend only on a single scale and are thus easier to compute. However, the denominators of the expanded propagators are now raised to higher powers. We use the program `rows` [20], which implements the so-called Laporta algorithm [21,22], to reduce all of these integrals to a small set of so-called master integrals. Compared to the calculation of the unpolarized decay rate and the helicity fractions, we do not encounter any new master integrals.

III. NUMERICAL RESULTS

Our analytical results can be found in the Appendix to this paper. For the numerical evaluation of the analytical expression we use the values $m_t = 173.1 \pm 0.6$ GeV, $m_W = 80.385 \pm 0.015$ GeV, and $\alpha_s^{(5)}(m_Z) = 0.1182 \pm 0.0012$ [23]. The strong coupling constant is then evolved to the required scale using five-loop running. Note that our result is expressed in terms of the strong coupling constant with six active flavors, whereas the initial value $\alpha_s^{(5)}(m_Z)$ is defined with only five. Thus, we also have to use the (four-loop) decoupling relation to translate the latter into the former. All of this is achieved with the help of version 3 of the program `RunDec` [24,25]. Our central value is $\alpha_s^{(6)}(m_t) = 0.1078$.

We present our results in terms of the reduced helicity rates $\hat{\Gamma}_\alpha$ defined by

$$\Gamma_\alpha = \frac{G_F m_t^3 |V_{tb}|^2}{8\sqrt{2}\pi} \hat{\Gamma}_\alpha. \tag{8}$$

The total unpolarized and polarized rates are denoted by $\alpha = U + L$ and $\alpha = (U + L)^P$, where L refers to the longitudinal and U to the unpolarized-transverse polarization of the W boson (the latter is the sum of the two transverse polarizations). We then expand the reduced rates up to the second order in the strong coupling constant α_s as

$$\hat{\Gamma}_\alpha^{\text{NNLO}} = \hat{\Gamma}_\alpha^{(0)} + \hat{\Gamma}_\alpha^{(1)}\left(\frac{\alpha_s}{\pi}\right) + \hat{\Gamma}_\alpha^{(2)}\left(\frac{\alpha_s}{\pi}\right)^2, \tag{9}$$

where $\alpha_s \equiv \alpha_s^{(6)}(m_t)$ is defined with six active flavors and evaluated at the renormalization scale $\mu = m_t$. Furthermore, we define the coefficients in the $x = m_W/m_t$ expansion by

$$\hat{\Gamma}_{U+L}^{\text{NNLO}} = \sum_{i=0}^{10} \hat{\Gamma}_i^{\text{NNLO}} x^i, \quad \hat{\Gamma}_{(U+L)^P}^{\text{NNLO}} = \sum_{i=0}^{10} \hat{\Gamma}_{P,i}^{\text{NNLO}} x^i. \tag{10}$$

For $\hat{\Gamma}_{U+L}^{(2)}$ we use the result of Ref. [14]. Note that the coefficients of $\hat{\Gamma}_{U+L}$ contain logarithms of x. In principle, the sums run up to infinity, but in practice we only calculated

TABLE I. Numerical values for coefficients in the x expansion of the unpolarized and polarized reduced rates $\hat{\Gamma}_{U+L}^{\text{NNLO}}$ and $\hat{\Gamma}_{(U+L)^P}^{\text{NNLO}}$ [cf. Eq. (10)]. The results for the rates are given in the last line. In the third and fourth column we list the values of the asymmetry parameter at NLO and NNLO at a given order n in the x expansion [cf. Eq. (11)].

n	$\hat{\Gamma}_n^{\text{NNLO}}$	$\hat{\Gamma}_{P,n}^{\text{NNLO}}$	$\alpha_P^{\text{NLO}}(n)$	$\alpha_P^{\text{NNLO}}(n)$
0	+0.88690	+0.88360	0.99671	0.99628
2	+0.07452	−3.65421	0.11502	0.10582
4	−2.93225	+4.93143	0.42533	0.42381
5	0	−0.31636	0.41792	0.41490
6	+2.02534	−2.08447	0.38221	0.37763
7	0	+0.23471	0.38338	0.37901
8	−0.15921	−0.00614	0.38351	0.37916
9	0	+0.01129	0.38352	0.37918
10	−0.03276	−0.00048	0.38352	0.37919
$\hat{\Gamma}_\alpha^{\text{NNLO}}$	+0.78655	+0.29825		

the terms up to $\mathcal{O}(x^{10})$. This is sufficient to provide a reliable approximation of the full result. Up to the order $\mathcal{O}(x^n)$ we then calculate the NLO and NNLO values of the asymmetry parameter according to the ratio

$$\alpha_P^{\text{(N)NLO}}(n) = \frac{\sum_{i=0}^n \hat{\Gamma}_{P,i}^{\text{(N)NLO}} x^i}{\sum_{i=0}^n \hat{\Gamma}_i^{\text{(N)NLO}} x^i}, \tag{11}$$

where $\hat{\Gamma}_\alpha^{\text{NLO}}$ is defined as in Eq. (9), but with $\hat{\Gamma}_\alpha^{(2)}$ set to zero.

In Table I we give numerical results for the coefficients of the reduced rates and the asymmetry parameter. Analytical results are given in the Appendix. For the reduced rates, we find that the absolute values of the coefficients in the power series in x decrease when the power of x increases. The convergence of the x expansion is also illustrated in Figs. 2 and 3. Figure 2 shows the $\mathcal{O}(\alpha_s)$ and $\mathcal{O}(\alpha_s^2)$ contributions to $\hat{\Gamma}_{(U+L)^P}^{\text{NNLO}}$ as functions of x. We observe in both cases that adding terms beyond x^6 leads only to small changes at the physical value of x. Furthermore, the results truncated after x^8 and x^{10} are visually indistinguishable even up to $x = 0.6$. A similar behavior can be observed for α_P^{NNLO} in Fig. 3. (The figure for α_P^{NLO} would look very similar due to the smallness of the $\mathcal{O}(\alpha_s^2)$ correction.) Finally, we note that the unexpanded result for $\hat{\Gamma}_{(U+L)^P}^{(1)}$ given in the Appendix would be indistinguishable from the $n = 10$ curve in the upper panel of Fig. 2. Thus, we have good convergence behavior, and the truncation of the series does not change the result for all practical purposes. Indeed, we can see in Table I that the difference between $\alpha_P^{\text{(N)NLO}}(10)$ and $\alpha_P^{\text{(N)NLO}}(8)$ at the physical value for x is already at the level of 10^{-5}.

In order to determine the precision of our final result for the asymmetry parameter, we consider the following sources of uncertainties:
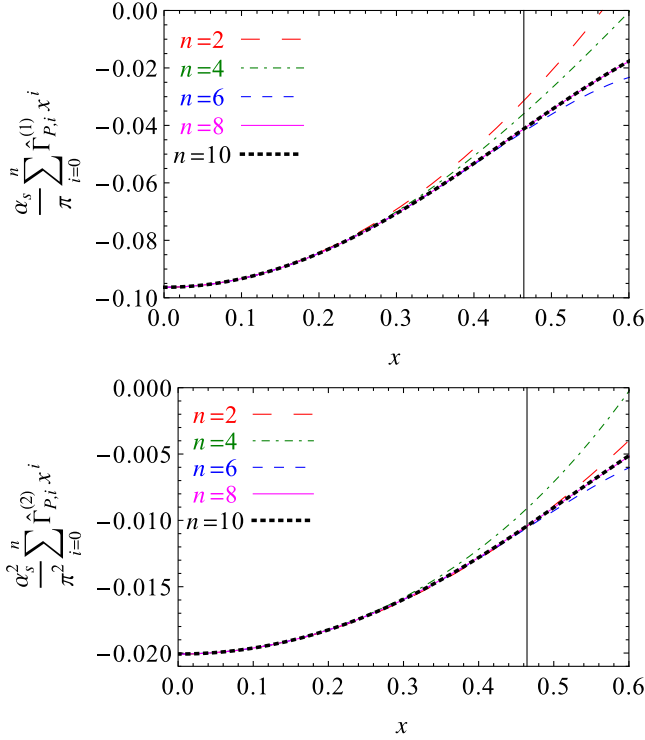
FIG. 2. The $\mathcal{O}(\alpha_s)$ and $\mathcal{O}(\alpha_s^2)$ contributions to $\hat{\Gamma}^{\text{NNLO}}_{(U+L)^P}$ as functions of x. The coefficients $\hat{\Gamma}^{(k)}_{P,i}$ are defined analogously to the ones in Eq. (10), but for $\hat{\Gamma}^{(k)}_{(U+L)^P}$ instead of $\hat{\Gamma}^{\text{NNLO}}_{(U+L)^P}$. Our central value for $\alpha_s^{(6)}(m_t)$ is used throughout. The vertical line indicates the physical value of x. Note that the lines for $n = 8$ lie below the ones for $n = 10$.
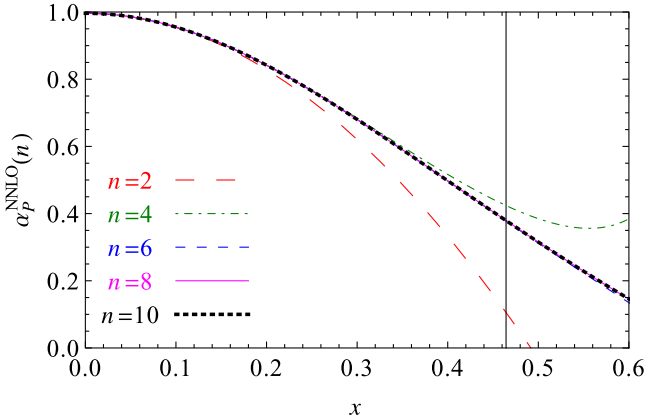
FIG. 3. $\alpha_P^{\text{NNLO}}(n)$ as a function of x. Our central value for $\alpha_s^{(6)}(m_t)$ is used throughout. The vertical line indicates the physical value of x. Note that the lines for $n = 6$ and $n = 8$ lie below the one for $n = 10$.

(i) The uncertainty in the mass of the top quark. This is the largest source of uncertainty in our result. We note that in our calculation we have employed the pole mass definition for the top quark, whereas

the numerical value corresponds to the so-called Monte-Carlo mass parameter. This difference adds an additional uncertainty to our result, which is, however, currently not precisely known and not included in our analysis. (Recent efforts to determine this difference can be found in Refs. [26,27].)

(ii) Higher orders in QCD. We estimate the size of unknown higher order corrections by taking half the difference between $\alpha_P^{\text{NNLO}}(10)$ and $\alpha_P^{\text{NLO}}(10)$.[2]

(iii) The strong coupling constant. In addition to the uncertainty in the value of $\alpha_s^{(5)}(m_Z)$, we also vary the decoupling scale at which the five-flavor value is translated to the six-flavor one. However, the effect of the latter is completely negligible.

(iv) The uncertainty in the mass of the W boson.

(v) The truncation of the series in x. We estimate this effect by taking the difference between $\alpha_P^{\text{NNLO}}(10)$ and $\alpha_P^{\text{NNLO}}(8)$. As can be seen from Table I, this uncertainty is very small.

(vi) Nonzero bottom-quark mass. We estimate the error due to setting m_b to zero by taking the difference to $\alpha_P^{\text{NNLO}}(10)$ computed as before, but with $m_b = 5$ GeV in the Born-level contributions $\hat{\Gamma}^{(0)}_{U+L}$ and $\hat{\Gamma}^{(0)}_{(U+L)^P}$.

Our final result is

$$\alpha_P^{\text{NNLO}} = 0.3792 \pm 0.0029(m_t) \pm 0.0022(\text{higher orders})$$
$$\pm 0.0002(\alpha_s) \pm 0.0002(m_W)$$
$$\pm 0.00002(\text{truncation})$$
$$\pm 0.0004(m_b \neq 0) \tag{12}$$

$$= 0.3792 \pm 0.0037. \tag{13}$$

In the last line, we have added the different uncertainties in quadrature. It is important to note that the above result includes only QCD corrections. However, at this level of precision, electroweak corrections can also play a role. Since the electroweak NLO corrections to $\hat{\Gamma}_{(U+L)^P}$ are currently unknown, we make an estimate of their size by looking at the known corrections to the helicity fractions, where they increase the Born-level results by roughly 2% [28]. The total decay rate is shifted by a similar amount [29,30]. Taking both of these corrections into account changes our result for α_P^{NNLO} only at the permille level, which is well within our uncertainty estimate.

IV. SUMMARY AND OUTLOOK

We have presented analytical and numerical results on the NNLO coefficients of a power series expansion of the

---

[2]Alternatively, one could also vary the renormalization scale by a factor two around the central value $\mu = m_t$. This would give a value that is roughly one half of the one from our chosen method.

polarized decay rate where we have expanded in the mass ratio $x = m_W/m_t$. Including the previously calculated LO and NLO results and the NNLO result for the unpolarized decay rate, we obtain a $\mathcal{O}(\alpha_s^2)$ result for the asymmetry parameter α_P determining the angular decay distribution of a polarized top quark decay. It would be interesting to experimentally check on the size of the asymmetry parameter in polarized top quark decays.

It is interesting to observe that the power series expansion of the parity-odd polarized rate $\hat{\Gamma}_P^{(i)}$ contains both even and odd powers while the parity-even unpolarized rate contains only even powers of x. This follows the pattern observed in the NNLO calculation of the helicity fractions [16]. We regret to say that we are lacking a deep understanding of this pattern. We mention that the electroweak NLO corrections to the structure functions do not follow this pattern.

In this paper we have summed over the three helicities of the W boson. It would be interesting to repeat the calculation for the three helicity components of the W boson separately. The corresponding decay distribution is given by

$$\frac{1}{\hat{\Gamma}}\frac{d\hat{\Gamma}}{d\cos\theta_P d\cos\theta} = \frac{1}{2}\left\{\frac{3}{8}(1+\cos\theta)^2(\hat{\Gamma}_+ + \hat{\Gamma}_+^P P_t \cos\theta_P)\right.$$
$$+ \frac{3}{8}(1-\cos\theta)^2(\hat{\Gamma}_- + \hat{\Gamma}_-^P P_t \cos\theta_P)$$
$$\left. + \frac{3}{4}\sin^2\theta(\hat{\Gamma}_L + \hat{\Gamma}_L^P P_t \cos\theta_P)\right\}. \quad (14)$$

It should be clear that all three asymmetry parameters $\alpha_j^P = \hat{\Gamma}_j^P/\hat{\Gamma}_j$ $(j = +, -, L)$ must satisfy the positivity condition $|\alpha_j^P| \leq 1$.

The LO Born term values for the unpolarized and polarized structure functions are given by [31,32]

$$\hat{\Gamma}_+ = 0, \qquad \hat{\Gamma}_+^P = 0,$$
$$\hat{\Gamma}_- = 2x^2(1-x^2)^2, \qquad \hat{\Gamma}_-^P = -2x^2(1-x^2)^2,$$
$$\hat{\Gamma}_L = (1-x^2)^2, \qquad \hat{\Gamma}_L^P = (1-x^2)^2. \quad (15)$$

The LO asymmetry parameter α_j^P is undetermined for the transverse-plus rate and maximal for the transverse-minus and longitudinal rates. This has to be compared to the total LO asymmetry parameter $\alpha_P^{\text{LO}} = 0.398$, which is far from being maximal.

Including the NLO corrections, one obtains $|\alpha_j^{P,\text{NLO}}| < 1$ for all three asymmetry parameters [32]. This is very gratifying from the point of view that the $\mathcal{O}(\alpha_s)$ asymmetry parameters satisfy the necessary positivity condition $|\alpha_j^P| \leq 1$. We expect that the inclusion of NNLO results in the calculation of the asymmetry parameter will retain this feature.

APPENDIX: ANALYTICAL RESULTS

In this Appendix we provide the analytical results for the reduced rates defined in Eqs. (8) and (9).

1. LO Born term contributions

$$\hat{\Gamma}_{U+L}^{(0)} = (1-x^2)^2(1+2x^2),$$
$$\hat{\Gamma}_{(U+L)^P}^{(0)} = (1-x^2)^2(1-2x^2). \quad (A1)$$

2. NLO α_s-corrections

Using the techniques described in the paper, we calculate the NLO corrections in α_s in terms of a series expansion in the mass ratio $x = m_W/m_t$. One has

$$\hat{\Gamma}_{U+L}^{(1)} = C_F\left[\frac{5}{4} + \frac{3}{2}x^2 - 6x^4 + \frac{46}{9}x^6 - \frac{7}{4}x^8 - \frac{49}{300}x^{10} - 2(1-x^2)^2(1+2x^2)\zeta(2) + \left(3 - \frac{4}{3}x^2 + \frac{3}{2}x^4 + \frac{2}{5}x^6\right)x^4\ln x\right],$$

$$\hat{\Gamma}_{(U+L)^P}^{(1)} = C_F\left[-\frac{15}{4} - \frac{17}{8}x^4 - \frac{1324}{225}x^5 - \frac{31}{36}x^6 + \frac{48\,868}{11\,025}x^7 - \frac{23}{288}x^8 + \frac{884}{6615}x^9 - \frac{3}{100}x^{10} + (1+4x^2)\zeta(2)\right], \quad (A2)$$

where $C_F = (N_c^2 - 1)/(2N_c) = 4/3$ for $N_c = 3$ colors and ζ denotes the Riemann zeta function. These results can be compared with the x expansion of the closed form results calculated in Refs. [31,32]. One has

$$\hat{\Gamma}^{(1)}_{U+L} = C_F \left[\frac{1}{4}(1-x^2)(5+9x^2-6x^4) - 2x^2(1+x^2)(1-2x^2)\ln x - \frac{1}{2}(1-x^2)^2(5+4x^2)\ln(1-x^2) \right.$$

$$\left. - 2(1-x^2)^2(1+2x^2)\left(2\text{Li}_2(x) + 2\text{Li}_2(-x) + \ln x \ln(1-x^2) + \frac{\pi^2}{6} \right) \right],$$

$$\hat{\Gamma}^{(1)}_{(U+L)^P} = C_F \left[-\frac{1}{4}(1-x)^2(15+2x-5x^2-12x^3+2x^4) + (1+4x^2)\zeta(2) - \frac{1}{2}(1-x^2)^2(1-4x^2)\ln(1-x) \right.$$

$$\left. - \frac{1}{2}(1-x^2)(3-x^2)(1+4x^2)\ln(1+x) - 2(1-x^2)^2(1-2x^2)\text{Li}_2(x) + 2(2+5x^4-2x^6)\text{Li}_2(-x) \right], \quad \text{(A3)}$$

where Li_2 denotes the dilogarithm function. We have found agreement in this comparison.

3. NNLO α_s^2-CORRECTIONS

We present our results in terms of the color-flavor decomposition

$$\hat{\Gamma}^{(2)}_\alpha = C_F[C_F\hat{\Gamma}^{(2F)}_\alpha + C_A\hat{\Gamma}^{(2A)}_\alpha + N_L T_F \hat{\Gamma}^{(2L)}_\alpha + N_H T_F \hat{\Gamma}^{(2H)}_\alpha], \quad \text{(A4)}$$

where $C_A = N_c = 3$, $T_F = 1/2$, $N_L = 5$, and $N_H = 1$. The coefficients of $\hat{\Gamma}^{(2)}_{U+L}$ were calculated in Ref. [14] and are presented here for completeness. We have

$$\hat{\Gamma}^{(2F)}_{U+L} = 5 - \frac{73}{8}x^2 - \frac{7537}{288}x^4 + \frac{16499}{864}x^6 - \frac{1586479}{259200}x^8 - \frac{11808733}{6480000}x^{10} + \left(\frac{115}{24} - \frac{367}{72}x^2 + \frac{31979}{8640}x^4 + \frac{13589}{13500}x^6 \right)x^4 \ln x$$

$$- \left(\frac{119}{8} - \frac{123}{4}x^2 - \frac{523}{16}x^4 + \frac{407}{36}x^6 - \frac{2951}{1152}x^8 - \frac{37}{400}x^{10} - \left(\frac{57}{2} - \frac{81}{8}x^4 - 6x^6 \right)\ln 2 \right.$$

$$\left. + \left(\frac{15}{4} - \frac{20}{3}x^2 + \frac{3}{4}x^4 + \frac{1}{5}x^6 \right)x^4 \ln x \right)\zeta(2) - \left(\frac{53}{8} - \frac{295}{32}x^4 + \frac{7}{2}x^6 - \frac{9}{2}x^8 - \frac{6}{5}x^{10} \right)\zeta(3)$$

$$- \left(\frac{11}{8} + 41x^2 + \frac{191}{8}x^4 - \frac{21}{4}x^6 \right)\zeta(4),$$

$$\hat{\Gamma}^{(2F)}_{(U+L)^P} = -\frac{35}{48} - \frac{3245}{48}x^2 + \frac{132413}{11520}x^4 - \frac{6991909}{405000}x^5 + \frac{1931557}{72576}x^6 + \frac{13210017881}{972405000}x^7 - \frac{68041043843}{1219276800}x^8$$

$$+ \frac{92602080451}{35006580000}x^9 - \frac{4454582599}{14515200}x^{10} - \left(\frac{35}{4} - 61x^2 - \frac{1889}{32}x^4 - \frac{862}{75}x^5 - \frac{4529}{72}x^6 + \frac{87146}{11025}x^7 - \frac{1674161}{9216}x^8 \right.$$

$$\left. + \frac{31246}{19845}x^9 - \frac{122414357}{230400}x^{10} - \left(\frac{55}{2} - 19x^2 + \frac{93}{8}x^4 - \frac{1279}{16}x^6 - \frac{64787}{256}x^8 - \frac{24113}{32}x^{10} \right)\ln 2 \right)\zeta(2)$$

$$- \left(\frac{95}{8} - \frac{113}{4}x^2 + \frac{5927}{160}x^4 - \frac{70097}{1344}x^6 - \frac{11855441}{107520}x^8 - \frac{286453}{896}x^{10} \right)\zeta(3)$$

$$- \left(\frac{3}{8} + \frac{177}{4}x^2 + \frac{605}{8}x^4 + \frac{337}{4}x^6 + \frac{171}{2}x^8 + \frac{171}{2}x^{10} \right)\zeta(4) - 4(1-2x^2)(2-2x^2+x^4)\left(\text{Li}_4\left(\frac{1}{2}\right) - \ln^2 2\zeta(2) + \frac{1}{24}\ln^4 2 \right),$$

$$\hat{\Gamma}^{2A}_{U+L} = \frac{521}{576} + \frac{91}{48}x^2 - \frac{12169}{576}x^4 + \frac{13685}{864}x^6 - \frac{420749}{103680}x^8 - \frac{4868261}{12960000}x^{10} + \left(\frac{73}{8} - \frac{1121}{216}x^2 + \frac{11941}{3456}x^4 + \frac{153397}{108000}x^6 \right)x^4 \ln x$$

$$+ \left(\frac{505}{144} + \frac{329}{24}x^2 + \frac{2171}{96}x^4 - \frac{47}{12}x^6 - \frac{3263}{2304}x^8 - \frac{557}{800}x^{10} - \left(\frac{57}{4} - \frac{81}{16}x^4 - 3x^6 \right)\ln 2 \right.$$

$$\left. - \left(\frac{9}{8} + 2x^2 + \frac{9}{8}x^4 + \frac{3}{10}x^6 \right)x^4 \ln x \right)\zeta(2) + \left(\frac{9}{16} + \frac{377}{64}x^4 - \frac{19}{4}x^6 - \frac{9}{8}x^8 - \frac{3}{10}x^{10} \right)\zeta(3)$$

$$+ \left(\frac{11}{16} - \frac{39}{2}x^2 - \frac{385}{16}x^4 + \frac{43}{8}x^6 \right)\zeta(4),$$

$$\hat{\Gamma}^{2A}_{(U+L)^P} = -\frac{3155}{192} + \frac{15}{16}x^2 - \frac{5213}{384}x^4 - \frac{645\,811}{40\,500}x^5 + \frac{6\,888\,169}{259\,200}x^6 + \frac{19\,545\,586}{1\,929\,375}x^7 + \frac{7\,008\,567\,101}{101\,606\,400}x^8$$

$$+ \frac{8\,723\,471\,549}{26\,254\,935\,000}x^9 + \frac{117\,991\,469\,621}{609\,638\,400}x^{10} + \left(\frac{1129}{144} + \frac{455}{18}x^2 + \frac{3229}{192}x^4 + \frac{31}{225}x^5 + \frac{373}{144}x^6 - \frac{353}{735}x^7\right.$$

$$\left. - \frac{345\,851}{6144}x^8 + \frac{1853}{2835}x^9 - \frac{35\,471\,879}{153\,600}x^{10} - \left(\frac{55}{4} - \frac{19}{2}x^2 + \frac{93}{16}x^4 - \frac{1279}{32}x^6 - \frac{64\,787}{512}x^8 - \frac{24\,113}{64}x^{10}\right)\ln 2\right)\zeta(2)$$

$$+ \left(\frac{191}{16} - \frac{427}{24}x^2 + \frac{6329}{192}x^4 - \frac{4909}{128}x^6 - \frac{12\,031\,441}{215\,040}x^8 - \frac{4\,301\,531}{26\,880}x^{10}\right)\zeta(3)$$

$$- \left(\frac{9}{4} + \frac{117}{8}x^2 + \frac{531}{16}x^4 + \frac{373}{8}x^6 + \frac{93}{2}x^8 + \frac{93}{2}x^{10}\right)\zeta(4)$$

$$+ 2(1 - 2x^2)(2 - 2x^2 + x^4)\left(\mathrm{Li}_4\left(\frac{1}{2}\right) - \ln^2 2\zeta(2) + \frac{1}{24}\ln^4 2\right),$$

$$\hat{\Gamma}^{2L}_{U+L} = -\frac{4}{9} - \frac{19}{6}x^2 + \frac{745}{72}x^4 - \frac{5839}{648}x^6 + \frac{4253}{8640}x^8 - \frac{689}{27\,000}x^{10} - \left(\frac{7}{2} - \frac{10}{3}x^2 + \frac{17}{72}x^4 + \frac{7}{450}x^6\right)x^4\ln x$$

$$+ \left(\frac{23}{18} + \frac{4}{3}x^2 - \frac{31}{6}x^4 + \frac{14}{9}x^6 + \frac{3}{2}x^8 + \frac{2}{5}x^{10}\right)\zeta(2) + (1 - x^2)^2(1 + 2x^2)\zeta(3),$$

$$\hat{\Gamma}^{2L}_{(U+L)^P} = \frac{19}{4} - \frac{1}{2}x^2 + \frac{1565}{288}x^4 + \frac{20\,249}{3375}x^5 + \frac{9319}{6480}x^6 - \frac{437\,779}{128\,625}x^7 - \frac{513\,487}{725\,760}x^8 - \frac{4\,993\,343}{12\,502\,350}x^9 - \frac{284\,003}{2\,268\,000}x^{10}$$

$$+ \left(\frac{10}{9} - \frac{44}{9}x^2 + \frac{5}{6}x^4 + \frac{8}{9}x^6 - \frac{7}{18}x^8 - \frac{4}{45}x^{10}\right)\zeta(2) - \left(3 - \frac{4}{3}x^2 + \frac{25}{3}x^4 - \frac{10}{3}x^6\right)\zeta(3),$$

$$\hat{\Gamma}^{2H}_{U+L} = \frac{12\,991}{1296} - \frac{35}{108}x^2 - \frac{6377}{432}x^4 + \frac{319}{27}x^6 + \frac{76\,873}{8640}x^8 + \frac{237\,107}{27\,000}x^{10}$$

$$- \left(\frac{53}{9} + \frac{8}{3}x^2 - \frac{25}{3}x^4 + \frac{62}{9}x^6 + \frac{16}{3}x^8 + \frac{16}{3}x^{10}\right)\zeta(2) - \left(\frac{1}{3} - 4x^2 - x^4 + \frac{2}{3}x^6\right)\zeta(3),$$

$$\hat{\Gamma}^{2H}_{(U+L)^P} = \frac{12\,991}{1296} - \frac{79}{81}x^2 + \frac{15\,197}{1296}x^4 - \frac{5005}{324}x^6 - \frac{328\,061}{25\,920}x^8 - \frac{2\,032\,763}{162\,000}x^{10}$$

$$- \left(\frac{53}{9} + \frac{28}{9}x^2 + \frac{109}{9}x^4 - \frac{10}{3}x^6 - \frac{16}{9}x^8 - \frac{16}{9}x^{10}\right)\zeta(2) - \left(\frac{1}{3} - \frac{16}{3}x^2 - \frac{19}{3}x^4 - \frac{26}{3}x^6 - 8x^8 - 8x^{10}\right)\zeta(3), \quad \text{(A5)}$$

where $\mathrm{Li}_4\left(\frac{1}{2}\right) = \sum_{i=1}^{\infty}\frac{1}{2^n n^4}$.

---

[1] M. Aaboud *et al.* (ATLAS Collaboration), Measurement of the inclusive cross-sections of single top-quark and top-antiquark *t*-channel production in *pp* collisions at $\sqrt{s} = $ 13 TeV with the ATLAS detector, J. High Energy Phys. 04 (2017) 086.

[2] M. Aaboud *et al.* (ATLAS Collaboration), Fiducial, total and differential cross-section measurements of *t*-channel single top-quark production in *pp* collisions at 8 TeV using data collected by the ATLAS detector, Eur. Phys. J. C **77**, 531 (2017).

[3] A. M. Sirunyan *et al.* (CMS Collaboration), Cross section measurement of *t*-channel single top quark production in pp collisions at $\sqrt{s} = $ 13 TeV, Phys. Lett. B **772**, 752 (2017).

[4] CMS Collaboration, Measurement of the differential cross section for *t*-channel single-top-quark production at $\sqrt{s} = $ 13 TeV, Report No. CMS-PAS-TOP-16-004, https://cds.cern.ch/record/2151074/files/TOP-16-004-pas.pdf.

[5] N. Faltermann, Single top *t*-channel in ATLAS and CMS, in *Proceedings for the Fifth Annual Large Hadron Collider Physics (LHCP2017) Conference, Shanghai, China, 2017* [arXiv:1709.00841].

[6] G. Mahlon and S. J. Parke, Single top quark production at the LHC: Understanding spin, Phys. Lett. B **476**, 323 (2000).

[7] T. M. P. Tait and C. P. Yuan, Single top quark production as a window to physics beyond the standard model, Phys. Rev. D **63**, 014018 (2000).

[8] D. Espriu and J. Manzano, Measuring effective electroweak couplings in single top production at the LHC, Phys. Rev. D **65**, 073005 (2002).

[9] D. Espriu and J. Manzano, A study of top polarization in single top production at the CERN LHC, Phys. Rev. D **66,** 114009 (2002).

[10] S. Groote, J. G. Körner, B. Melić, and S. Prelovsek, A survey of top quark polarization at a polarized linear e^+e^- collider, Phys. Rev. D **83,** 054018 (2011).

[11] E. L. Berger, J. Gao, C. P. Yuan, and H. X. Zhu, NNLO QCD corrections to t-channel single top-quark production and decay, Phys. Rev. D **94,** 071501 (2016).

[12] E. L. Berger, J. Gao, and H. X. Zhu, Differential distributions for t-channel single top-quark production and decay at next-to-next-to-leading order in QCD, J. High Energy Phys. 11 (2017) 158.

[13] I. R. Blokland, A. Czarnecki, M. Ślusarczyk, and F. Tkachov, Heavy to Light Decays with a Two Loop Accuracy, Phys. Rev. Lett. **93,** 062001 (2004).

[14] I. R. Blokland, A. Czarnecki, M. Ślusarczyk, and F. Tkachov, Next-to-next-to-leading order calculations for heavy-to-light decays, Phys. Rev. D **71,** 054004 (2005); Erratum, Phys. Rev. D **79,** 019901E (2009).

[15] I. R. Blokland, Multiloop calculations in perturbative quantum field theory, PhD thesis, University of Alberta, 2004, http://www.augustana.ualberta.ca/files/group/567/diss2.ps.

[16] A. Czarnecki, J. G. Körner, and J. H. Piclum, Helicity fractions of W bosons from top quark decays at NNLO in QCD, Phys. Rev. D **81,** 111503 (2010).

[17] D. Kreimer, The γ_5 problem and anomalies: A clifford algebra approach, Phys. Lett. B **237,** 59 (1990).

[18] J. G. Körner, D. Kreimer, and K. Schilcher, A Practicable γ_5 scheme in dimensional regularization, Z. Phys. C **54,** 503 (1992).

[19] V. A. Smirnov, Applied asymptotic expansions in momenta and masses, Springer Tracts Mod. Phys. **177,** 1 (2002).

[20] A. Pak (unpublished).

[21] S. Laporta and E. Remiddi, The Analytical value of the electron $g-2$ at order α^3 in QED, Phys. Lett. B **379,** 283 (1996).

[22] S. Laporta, High precision calculation of multiloop Feynman integrals by difference equations, Int. J. Mod. Phys. A **15,** 5087 (2000).

[23] C. Patrignani *et al.* (Particle Data Group), Review of particle physics, Chin. Phys. C **40,** 100001 (2016).

[24] K. G. Chetyrkin, J. H. Kühn, and M. Steinhauser, RunDec: A Mathematica package for running and decoupling of the strong coupling and quark masses, Comput. Phys. Commun. **133,** 43 (2000).

[25] F. Herren and M. Steinhauser, Version 3 of RunDec and CRunDec, Comput. Phys. Commun. **224,** 333 (2018).

[26] M. Butenschön, B. Dehnadi, A. H. Hoang, V. Mateu, M. Preisser, and I. W. Stewart, Top Quark Mass Calibration for Monte Carlo Event Generators, Phys. Rev. Lett. **117,** 232001 (2016).

[27] B. Dehnadi, A. H. Hoang, V. Mateu, M. Preisser, and I. W. Stewart, Monte Carlo Top Quark Mass Calibration, Proc. Sci. RADCOR2017 (**2018**) 062.

[28] H. S. Do, S. Groote, J. G. Körner, and M. C. Mauser, Electroweak and finite width corrections to top quark decays into transverse and longitudinal W bosons, Phys. Rev. D **67,** 091501 (2003).

[29] A. Denner and T. Sack, The top width, Nucl. Phys. **B358,** 46 (1991).

[30] G. Eilam, R. R. Mendel, R. Migneron, and A. Soni, Radiative Corrections to Top Quark Decay, Phys. Rev. Lett. **66,** 3105 (1991).

[31] M. Fischer, S. Groote, J. G. Körner, M. C. Mauser, and B. Lampe, Polarized top decay into polarized W: $t(\text{polarized}) \to W(\text{polarized}) + b$ at $O(\alpha_s)$, Phys. Lett. B **451,** 406 (1999).

[32] M. Fischer, S. Groote, J. G. Körner, and M. C. Mauser, Complete angular analysis of polarized top decay at $O(\alpha_s)$, Phys. Rev. D **65,** 054036 (2002).

[33] J. A. M. Vermaseren, New features of FORM, arXiv:math-ph/0010025.